Fuel Processing Technology 119 (2014) 1–9

Contents lists available at ScienceDirect

Fuel Processing Technology

journal homepage: www.elsevier.com/locate/fuproc

Experimental study of the spray characteristics of USLD, methanol and DME on the swirl nozzle of a Stirling engine

Wugao Zhang [a,*], Xiaoling Chen [a,*], Genxiang Gu [b], Huaili Hu [a], Taotao Liu [a], Zhen Huang [a]

[a] Key Laboratory for Power Machinery and Engineering of the Ministry of Education, Shanghai Jiao Tong University, Shanghai 200240, China
[b] Micropowers Ltd., Shanghai 200233, China

ARTICLE INFO

Article history:
Received 2 January 2013
Received in revised form 1 October 2013
Accepted 7 October 2013
Available online 13 November 2013

Keywords:
Stirling engine
Methanol
DME
ULSD
Spray characteristics
Size distribution characteristics

ABSTRACT

The objective of this paper was to investigate the spray characteristics of methanol and dimethyl ether (DME) on the swirl nozzle of a Stirling engines by comparing with traditional ultralow sulfur diesel fuels (USLD) under different fuel injection rates and different surrounding back pressures in a constant volume pressure vessel. Under the test rig, the macroscopic and microscopic spray characteristics of the fuels were studied by a high speed camera and FAM Laser Particle Size Analyzer during the atomization process. The experimental results show that injection pressure and ambient pressure have a significant impact on the spray tip penetration and spray angles. Higher spray pressure makes the formation period of spray decrease and the penetration rate increase whereas higher back pressure inside the injection chamber leads to the shrinking of the spray angle. The atomization quality of DME under atmospheric back pressure is much better than that of methanol and ULSD while it becomes worse when ambient back pressure is higher than the saturated vapor pressure. Additionally, higher back pressure and a larger injection flow rate are beneficial to the atomization quality of ULSD, whereas those factors seem to have relatively small influence on the droplet size distribution of methanol.

Crown Copyright © 2013 Published by Elsevier B.V. All rights reserved.

1. Introduction

To alleviate the pressure of energy shortage and environmental problems caused by fossil fuels, two approaches are generally adopted: one is to enhance the energy utilization efficiency of fossil fuels by improving the operating methods and combustion quality of engines; the other is to look for new alternatives of fossil fuels to reduce pollution. The Stirling engine is an external combustion engine and is famous for its high efficiency (up to 40%), quiet operation, and the ease with which it can use almost any heat sources. Its compatibility with alternative energy sources has become increasingly significant, with the concerns on the shortage of conventional fuels, environmental pollution and climate change due to the consumption of fossil fuels.

The Stirling engine has been used typically in the military field, especially as the power generator of the AIP (air independent propulsion) system. Because of its compatibility with alternative fuels and renewable energy resources, this engine is starting to be used for civilian purposes, especially as the core component of micro combined heat and power (CHP) units, in which it is more efficient and safer than a steam engine. Katsura et al. (2008) [1] developed a 55 kWe Stirling engine CHP system and studied its biomass combustion performance of pulverized wood powder, while Akio [2] studied the fuel properties and emissions characteristics of a Stirling engine operated with wood powder. Ahmad (2011) [3] presented a detailed description of the performance and efficiency of a biogas CHP system utilizing a Stirling engine. Amir et al. (2009) [4] experimentally examined the performance of a residential micro cogeneration system based on a Stirling engine fueled by diesel and biodiesel while, Nicolas et al. (2012) [5] examined the performance of a micro cogeneration system based on a Stirling engine fueled by diesel and ethanol.

Energy and environmental issues caused by fossil fuel combustion have prompted a growing number of researchers to explore the application of alternative fuels. Under this background, this paper experimentally studies the spray characteristics of the Stirling engine using methanol, and dimethyl ether (DME) by comparing them with the traditional fuel of ultra-low sulfur diesel (ULSD). Methanol and DME both have rich resources and can reduce emissions (CO, HC, NOX, and PM) [6–13] during the combustion process, and they are considered as promising alternative fuels. However, the densities of methanol and DME are less than that of low sulfur diesel. At room temperature (20 °C), the kinematic viscosities of methanol and DME are less than one tenth of that of ULSD. The saturation vapor pressure of DME under room temperature is much higher than atmospheric pressure [14]. All those physical properties have a great impact on fuel spray formation, atomization characteristics, combustion and emissions. Because the Stirling engine performs continuous combustion, it is crucial to ensure the power output in a stable range by keeping the stability of heat release during the combustion process. To optimize the

* Corresponding authors. Tel./fax: +86 21 34206540.
E-mail addresses: zhangwg@sjtu.edu.cn (W. Zhang), xlchen@sjtu.edu.cn (X. Chen).

0378-3820/$ – see front matter. Crown Copyright © 2013 Published by Elsevier B.V. All rights reserved.
http://dx.doi.org/10.1016/j.fuproc.2013.10.006

combustion quality, it is important to improve the atomization quality of the Stirling engine. However, we will not comment on the combustion characteristics of fuels in this paper.

A practical pressure-swirl injector used in Stirling engines is operated here to study the spray characteristics of ULSD, methanol and DME. Very little information is available from literature on the penetration of diesel or biodiesel sprays from pressure-swirl injectors [15]. Wang et al. (1987) [16] only measured the mean drop size of diesel in pressure-swirl nozzles for different flow numbers and injection pressures. Wang et al. (2005) [17] measured the spray penetrations and cone angles of pressure-swirl injectors fueled with methanol and ethanol. Most investigations on spray characteristics of DME were conducted on a common-rail injection system with the injection pressure higher than 40 MPa [11,18,19]. Little information is about the flash-boiling sprays of volatile fuels (e.g. DME) actuated from the pressure-swirl injector with lower injection pressure (<10 MPa). Only the spray penetrations and cone angles of liquefied petroleum gas (LPG) at different back pressures were analyzed by Mesman et al. (2009) [20].

Above all, in this study, the macroscopic and microscopic spray characteristics of ultra low sulfur diesel (USLD), methanol and DME conducted on a pressure-swirl injector of a Stirling engine were investigated. The test rig is mainly composed of a constant-volume pressure vessel with a wide field of view, an oil supply system regulated by a high pressure cylinder, a high-speed video camera, a FAM laser particle size analyzer, image-processing software and a data acquisition system. The macroscopic spray characteristics including spray penetration, spray cone angle and spray tip penetration rate of three different fuels were measured by a high speed camera and analyzed based on their physico-chemical properties. The microscopic spray characteristics, such as droplet size distributions, were measured and analyzed by using a laser particle size analyzer.

2. Spray test system

2.1. Spray visualization experimental test rig

The schematic diagram of the Stirling engine spray test rig is shown in Fig. 1. The test rig is mainly composed of the constant-volume pressure vessel (Fig. 2) and the fuel injection system. The pressure vessel is made of stainless steel with the wall thickness of 60 mm to simulate the high-pressure condition inside the engine combustion chamber. It

Fig. 2. The high-pressure spray visualization chamber.

consists of three 100 × 150 mm transparent observation windows made of quartz and the designed maximum working pressure is 3.2 MPa. The injector is installed on the top of this vessel and a pressure sensor is installed on its top to monitor the pressure inside the vessel to monitor the real-time pressure of the container. The bottom of the pressure vessel is lined with barbed wire and a sponge to absorb fuel droplets within the vessel to prevent air flow from disturbing the spray formation.

In the fuel injection system, a 40 L high pressure nitrogen cylinder is connected to provide constant injection pressure functioning in a similar way to the high-pressure injection system in internal combustion engines. A 10 L capacity nitrogen gas cylinder with a permitted pressure of 20 MPa is adopted as an oil tank, which is equipped with a pressure gauge and a pressure relief valve to display and control the gas pressure inside the tank. In practice, a 10 L nitrogen gas cylinder is connected to the high pressure nitrogen vessel as a pressure stabilizer to alleviate the

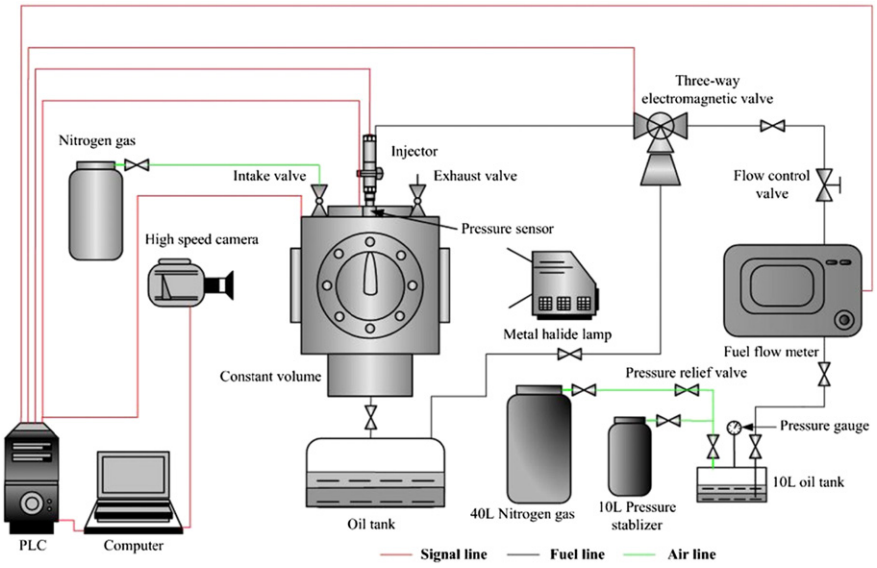

Fig. 1. Schematic diagram of the experimental setup.

Table 1
Physico-chemical of characteristics of samples and spray condition.

List	ULSD	Methanol	DME
Density (g/L,20 °C)	823	792	661
Kinematic viscosity ($mm^2 s^{-1}$, 20 °C)	9.03	0.70	0.15
Surface tension (N/m)	0.031	0.023	0.012
Boiling point (°C, 1 bar)	268~331	64.7	−24.9
Low heating value (MJ/kg)	43.04	19.92	28.80
Vapor pressure (bar, 20 °C)	0.00255	0.129	5.256

pressure fluctuations caused by the increasing residual space in the oil tank due to the fuel consumption. A three-way solenoid valve is used to control fuel injection which is quite different from the needle injector used in gasoline direct injection (GDI) engines. All the signals will be collected and transmitted to the programmable logic controller (PLC) system via a Labview man–machine interface and displayed on the computer screen, which in turn controls the three-way solenoid valve.

A high speed camera (FASTCAM-ultima APX 120KC) is used to record the spray pictures with a metal halide lamp as the light source. According to the fuel injection rate, the frame rate is 1000 frames per second and the image resolution is 512 × 1024. To facilitate the measurements, the pressure vessel is rinsed after 40 injection events. A laser particle size analyzer based on Fraunhofer and Mie (FAM) theory is used to measure the droplet size distribution of the spray.

2.2. The physico-chemical properties of testing fuels

The application of alternative fuels in engines faces many challenges because of their different physical and chemical properties and characteristics from conventional fuels. For example, density, viscosity, surface tension and volatility significantly influence the atomization, evaporation process and air/fuel ratio, and further affect the combustion and emissions. Some of the physico-chemical characteristics of methanol and DME are very different from the traditional fuel of ULSD used in Stirling engines, which will certainly influence the macroscopic and microscopic spray characteristics. The main physico-chemical characteristics of these fuels are listed in Table 1. It can be seen that the viscosities and surface tensions of methanol and DME are much lower compared to ULSD. DME has the lowest surface tension among the three fuels and its boiling point under atmospheric pressure (1 bar) is only −24.9 °C. The superheat temperature ($\Delta T_{sh} = T_{fuel} - T_{sat}$) of DME under room temperature (20 °C) is around 45 °C, which causes the flash boiling of DME under atmospheric pressure [20]. In the study, the nitrogen gas is charged into the pressure vessel to generate different back pressures.

2.3. Characteristics of the nozzle

Different from a typical pressure-swirl atomizer for GDI engines, a practical pressure-swirl nozzle used in the Stirling engine is operated to study the spray characteristics of ULSD, methanol and DME. In the interior of the nozzle there is a spiral flow channel where the high pressure liquid is forced through. After it flows through a small buffer chamber, it enters into four helical channels and a vortex chamber, which is designed to form a swirl flow to enhance the fuel atomization. Finally the liquid is ejected through a single hole with a diameter of 0.39 mm and nozzle orifice length of 0.5 mm. Fig. 3a shows the relationship between injection pressures and the mass flow rates of three fuels injected into atmospheric condition. It can be observed that the mass flow rate increases linearly with injection pressure. Due to a much higher viscosity, the injection pressure for ULSD is higher than the other two fuels to reach the same injection flow rate under the atmospheric back pressure. For example, at the same flow rate of 16 kg/h, the Reynolds number of ULSD, methanol and DME are 1.9524×10^3, 2.6172×10^4 and 1.4634×10^5 respectively. The friction factor decreases with the increase of Re for the laminar flow [21]. Therefore, ULSD required a higher injection pressure to compensate for the energy loss due to the friction, to reach the same mass flow rate of methanol and DME.

Fig. 3b shows the influence of back pressures on mass flow behavior of ULSD, with increasing the square root of pressure drop ($\Delta P^{1/2}$). The effects of back pressures on the injection mass flow rates are similar. At the low injection mass flow rate of 8 kg/h (where the Re is low), the $\Delta P^{1/2}$ at $P_b = 2.8$ MPa is higher than that of $P_b = 0.1$ MPa, due to more friction loss caused by the slightly increased viscosity of ULSD at higher back pressures [22]. At a higher injection rate of 20 m/s, the Re is higher, where the effect of friction loss is less at different back pressures.

3. Experimental results and discussion

The macroscopic spray characteristics of three fuels are analyzed with different injection pressures and ambient pressures. For a specified fuel, to study the influence of ambient pressure, a series of tests were conducted by changing the ambient pressures under the same flow rate. For comparing the effect of the injection mass flow rate, the injection pressure was regulated under the same ambient pressure. Very limited information is available from the literature on the spray characteristics of ULSD, methanol and DME from pressure-swirl nozzles at our interested injection conditions, and the swirl chamber geometries were different from ours. However, we will try to compare the results in this study with the published references on the spray characteristics of diesel (Wang et al., 1987 [16]), alcohols (Wang et al., 2005 [17]) and LPG (Mesman et al., 2009 [20]) from a pressure-swirl nozzle.

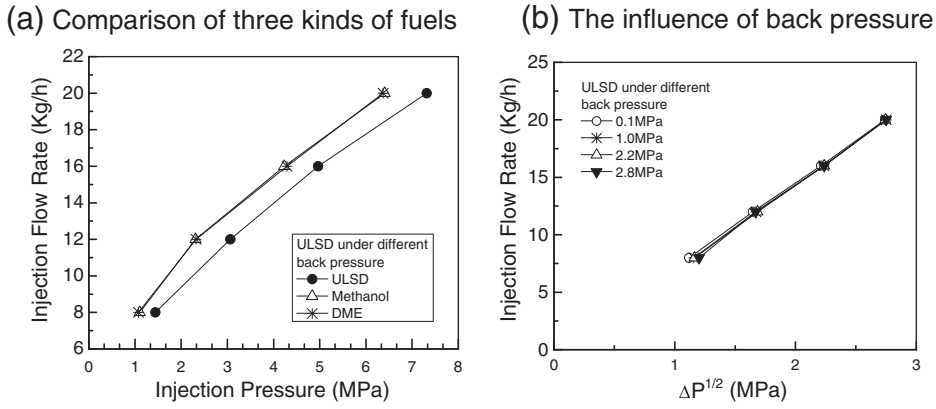

Fig. 3. Mass flow behavior of the nozzle.

3.1. Spray tip penetration

The spray tip penetration and near-field spray angle (defined as the angle between the tangents to the spray envelope in the region between 10 mm and 20 mm, extending from nozzle tip) [16] are identified by the GNU image manipulation program (GIMP) based on the calibrated pixels of digital images. Fig. 4a shows the spray tip penetration of ULSD under various back pressures (Pb = 0.1, 1.0 and 2.2 MPa) and a fixed injection flow rate of 16 kg/h. As shown, ULSD tip penetration develops quickly under higher back pressure conditions during the initial period of the injection whereas the penetration length of the fuel under lower back pressure exceeds that of higher back pressure during 16~20 ms. The maximum penetration difference between 0.1 MPa and 2.2 MPa is about 47 mm at 7 ms. This is mainly because higher back pressure means a higher gas density in the vessel, which inhibits the droplets from vaporizing and breaking into the surrounding fields. Under a back pressure of 2.2 MPa, the spray is compressed along a radial direction and the spray tip develops more quickly along the axial direction. At P_b = 0.1 MPa, as shown in Fig. 6a, the spray developed from a thin distorted pencil, onion stage, tulip stage to a fine atomization [15], which indicated a smaller cone angle at the start of injection.

Fig. 4b shows the influence of injection flow rates (8 kg/h,12 kg/h, 16 kg/h and 20 kg/h) on the spray tip penetration of ULSD at Pb = 0.1 MPa. It is evident that, during the initial period of injection, the lower mass flow rates have an obvious effect on the spray penetration indicating a period with lower penetration rates (14 ms, 11 ms, 7 ms for 8 kg/h, 12 kg/h, 16 kg/h respectively). The smaller injection mass flow rate means smaller initial momentum of the liquid jet, which has a relatively longer impact on the spray initial development. When the mass flow rate goes up to 20 kg/h, the initial period with lower penetration rate disappears and the penetration length increase linearly with injection time from the beginning.

Fig. 4c and b show a comparison of spray penetration of ULSD, methanol and DME when the injection flow rate is 16 kg/h and back pressures are 0.1 MPa and 2.2 MPa respectively. At P_b = 0.1 MPa (Fig. 4c), DME has the highest penetration rate, while the penetration rate of methanol is just a little higher than that of ULSD. The saturation vapor pressure of DME at room condition is much lower than atmospheric back pressure. The dimensionless ambient-to-saturation pressure ratio (Pa/Ps) of DME is 0.18 and its spray is in the extreme flash-boiling state where the spray penetration increases quickly with bubble growth and break up. The spray penetrations of methanol were measured by Wang et al. (2005) [17] from a pressure-swirl nozzle (Mitsubishi injector) under P_{inj} = 5.0 MPa and P_b = 0.1 MPa. The penetration rate of methanol is higher than that in our case during the first 5 ms, mainly due to different geometry of the injectors. The spray penetrations of LPG were measured by Mesman et al., 2009 [20] from a pressure-swirl nozzle (Siemens injector) under P_{inj} = 5.0 MPa and P_b = 0.1 MPa. Due to the higher injection pressure (P_{inj} = 5.0 MPa) and different injector types, the penetration rates were much higher than the other three fuels at P_b = 0.1 MPa.

Conversely, under a 2.2 MPa ambient pressure (Fig. 4d), ULSD has the longest penetration length and tip rate while DME has the lowest penetration rate during the first 10 ms. This phenomenon can be

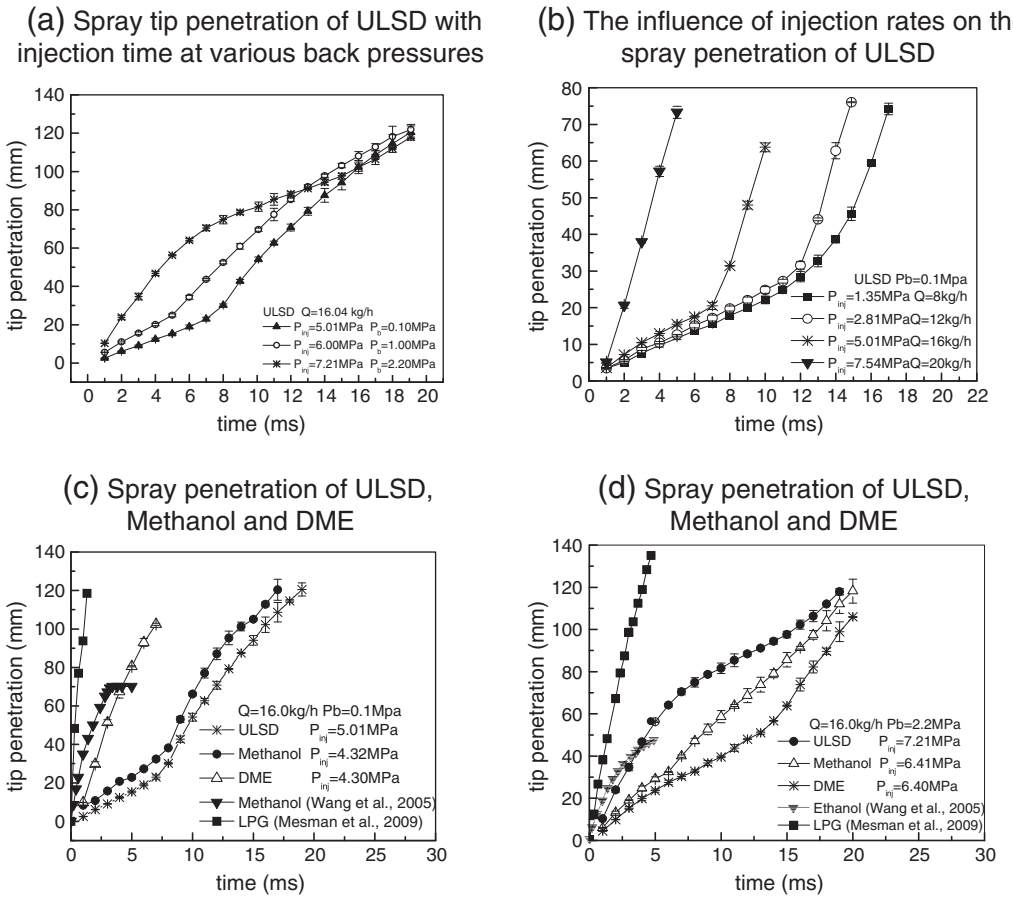

Fig. 4. a) Spray tip penetration of ULSD with injection time at various back pressures. b) The influence of injection rates on the spray penetration of ULSD. c) Spray penetration of ULSD, Methanol and DME. d) Spray penetration of ULSD, methanol and DME.

attributed to the difference of their physical properties. High back pressure keeps DME from boiling during the atomization. The difference of viscosity and surface tension affects the fuel/air mixing leading to the difference of spray penetration during the spray initial period. With the development of spray, the tip penetrations of the three fuels are approaching similarly. The spray penetrations of ethanol were measured by Wang et al. (2005) [17] from a pressure-swirl nozzle (Mitsubishi injector) under $P_{inj} = 5.0$ MPa and $P_b = 2.0$ MPa. The penetration rate of ethanol is higher than that of methanol in our case during the first 5 ms, mainly due to a different geometry of injectors. Similarly, the spray penetrations of LPG were measured by Mesman et al., 2009 [20] from a pressure-swirl nozzle (Siemens injector) under $P_{inj} = 5.0$ MPa and $P_b = 1.0$ MPa. Due to the lower back pressure ($P_b = 1.0$ MPa), the penetration rates were much higher than the other three fuels at $P_b = 2.2$ MPa.

3.2. Spray cone angle

In our experiments, the spray cone angle is measured from the photo of the spray when the spray stays at relatively stable conditions (generally after 50 ms from the start of actuation). Fig. 5a shows spray photos of ULSD at 50 ms under various back pressures (Pb = 0.1, 1.0, 2.2 and 2.8 MPa) and a fixed injection rate of 16 ± 0.05 kg/h. From the photos, it can be seen that the spray density increases and spray cone angle decreases with the increase of ambient pressure. The higher ambient pressure exerts an obvious compression effect on the spray cone angles (64.9°, 58.2°, 52.9°, 44.1°, 40.8°for 0.1, 1.0, 2.2 and 2.8 MPa respectively). This can be explained by the jet momentum consumed along the radial direction during atomization being inhibited when the gas density of the chamber becomes denser due to higher back pressures, which further influences the air entrainment, atomization diffusion and even volatilization of the spray. With the increase of back pressure, the change of the spray cone angle becomes unobvious. It can be also seen that there are some large droplets around the spray envelop under ambient pressures of 2.2 MPa and 2.8 MPa. Such a phenomenon can be explained because when the back pressure increases to a certain value the influence of surface tension and viscosity decreases relatively and droplet coalescence which influences droplets dispersion begins to pose an important role.

Fig. 5b shows the influence of injection flow rates of ULSD on the spray cone angle (64.9, 68.5, 70.6, and 71.9 for 8.06, 12.02, 16.04, and 20.00 kg/h respectively) under $P_b = 0.1$ MPa within a 10 ms spray duration. It is evident that the spray cone angle increases with the increase of fuel flow rates. As the injection rate increases, the rate of the spray cone angle decreases. Generally, a higher injection flow rate means a higher flow velocity and centrifugal force caused by the spiral channel of the injector, leading to the enhanced air entrainment and droplet breakup. On the other hand, with the increment of the mass flow rate, a combination effect of air entrapment and centrifugal force makes droplet coalescence become stronger, which in turn limits the increase of the spray cone angle. In comparison to the influence of back pressures on the spray angles, the spray cone angle of ULSD is more sensitive to back pressures than injection flow rates.

Fig. 5c shows the spray cone angles of three kinds of fuels under $P_b = 2.20$ MPa and Q = 16 ± 0.05 kg/h. Under this spray condition, the mean spray cone angles of methanol and DME were 26.5 and 29.1 respectively. The difference between DME and ULSD was almost 8° on average when the spray reached a relatively stable condition. Although this comparison is under the same injection rate of 16 ± 0.05 kg/h

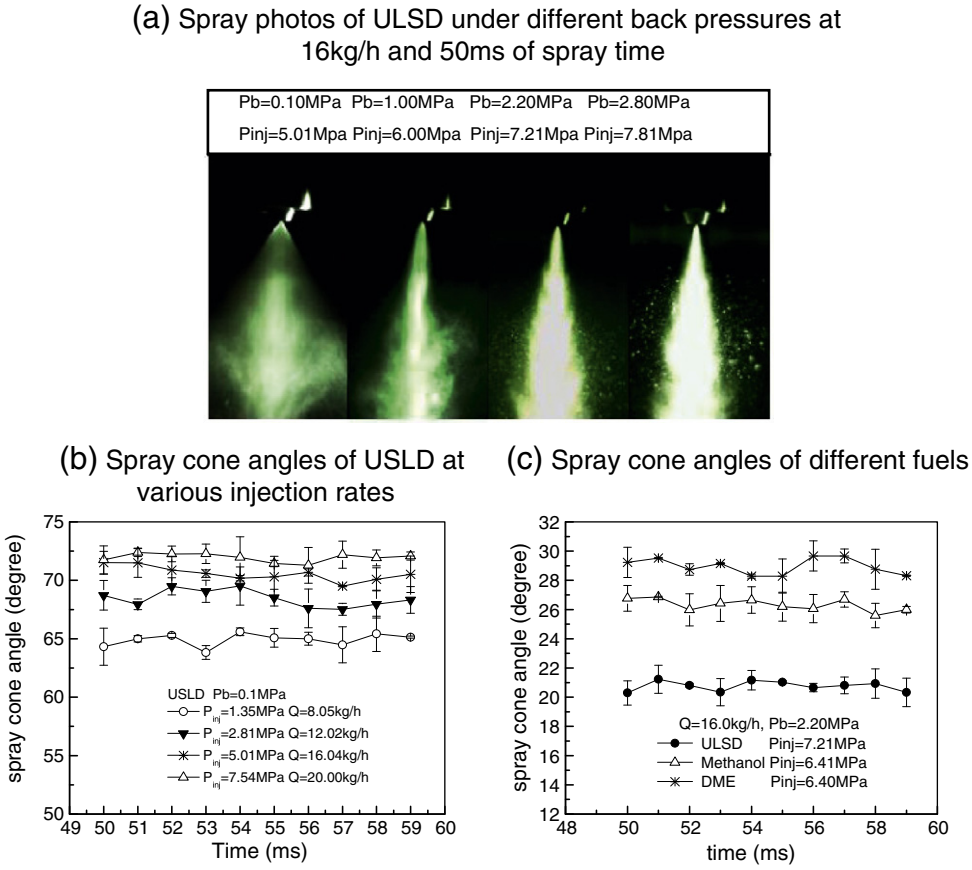

Fig. 5. a) Spray photos of ULSD under different back pressures at 16 kg/h and 50 ms of spray time. b) Spray cone angles of USLD at various injection rates. c) Spray cone angles of different fuels.

(P_b = 2.20 MPa), the bulk liquid velocity of DME and ULSD are 56.3 m/s and 45.2 m/s respectively because of their density difference. This velocity difference causes the radial and tangential velocities of DME to become larger than that of ULSD during the initial period of spray leading to a stronger radial mixing and thus a larger spray cone angle. The cone angle of LPG measured by Mesman et al., 2009 [20] at a relatively stable state under P_b = 1.0 MPa is 39.05°, which is higher than that of DME at P_b = 2.20 MPa due to lower back pressure.

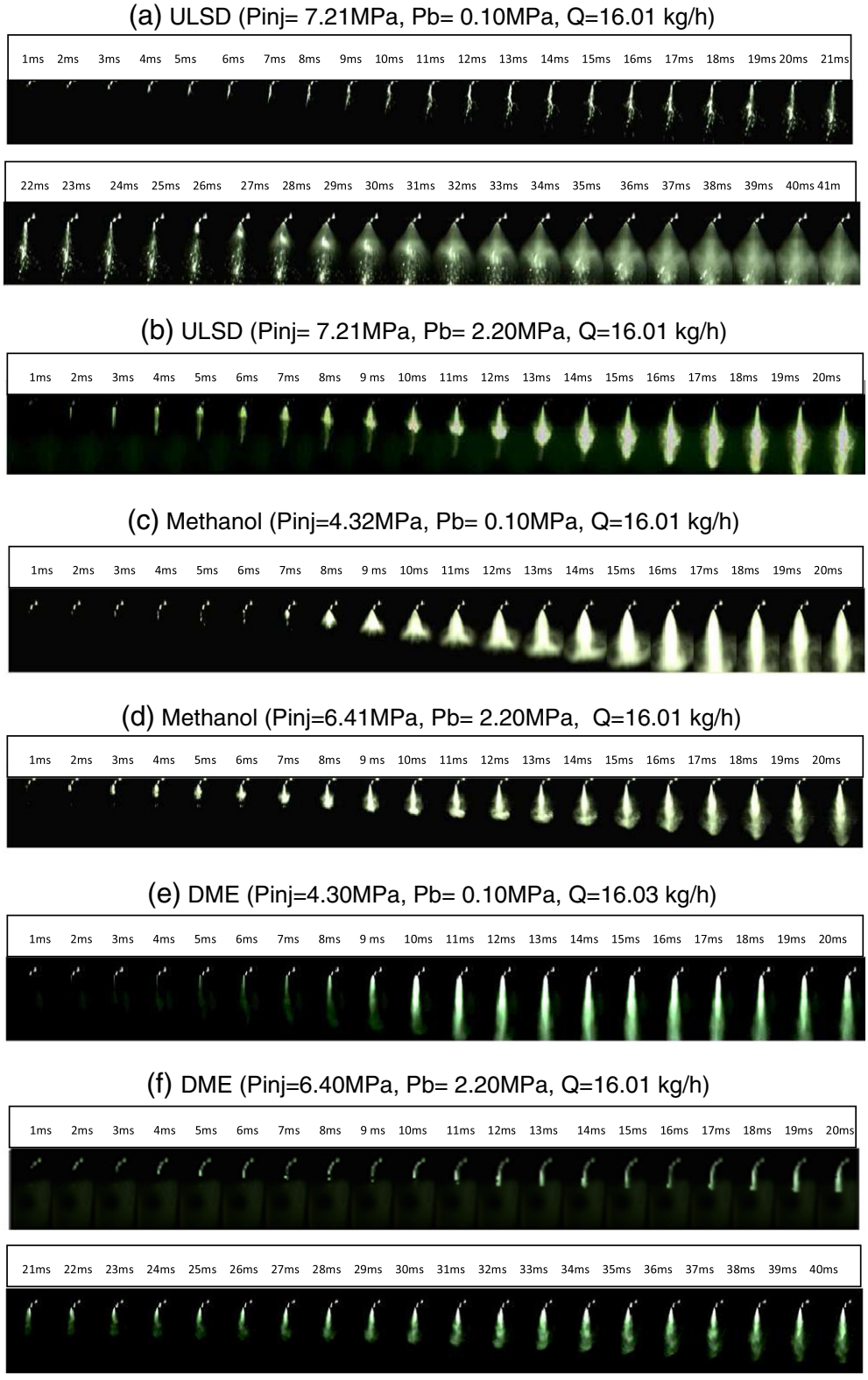

Fig. 6. The macroscopic spray images of ULSD, methanol and DME under different back pressures.

3.3. Spray morphology under high back pressure

Fig. 6 presents the macroscopic spray images of ULSD, methanol and DME under the back pressure of 0.1 MPa and 2.2 MPa respectively with a fuel flow rate of 16 kg/h from the start of injection. The difference of the three kinds of fuels during the atomization process and the influence of ambient pressures are demonstrated clearly from those photos. At $P_b = 0.1$ MPa, ULSD initially breaks into some ligaments and small droplets separate from the jet surface as distorted pencils [15]. This is due to the slower flow inside the nozzle at the beginning of injection when the fuel has not received sufficient rotational motion [23]. After about 25 ms, the spray begins to break up completely with a hollow cone and develops quickly indicating a better atomization. Furthermore, under higher back pressure ($P_b = 2.2$ MPa), the tip penetration and atomization are inhibited obviously as showed in Fig. 6b, especially from a radial direction. The atomization of methanol shows similar behavior under high ambient pressure. Under atmospheric pressure, the cone angles generated by the secondary gas flow [23] are much larger than those at $P_b = 2.2$ MPa. The DME under atmospheric pressure is in flash boiling condition and shows a very different atomization behavior with a quick penetration rate. Under 2.2 MPa, the penetration rate and atomization behavior of DME are depressed greatly (Fig. 6e,f). The differences of physical properties of ULSD, methanol and DME lead to the great difference of spray morphology.

3.4. Droplet size measurement

In this study, the FAM laser particle size analyzer was used to analyze particle size distribution. It can get the information of the particle size distribution along a laser line (the diameter of the cross-section of the line is 5 mm). For a complete spray, the particle size distribution is not the same at different locations. By changing the position of the FAM laser particle size analyzer, a complete spray distribution could be known about. All the results in this part are from a line perpendicular to the axial direction of the spray with an axial distance of a 112 mm from the nozzle. Rosin–Rammler accumulated droplets size distribution and Sauter mean diameter (SMD) are adopted to analyze the fuel atomization quality. Fig. 7 represents the accumulated percentages and overall SMD of ULSD droplets with the flow rate of 8 kg/h and under different back pressures. It can be seen that the droplet size is smaller and the distribution is more homogeneous at a back pressure of 1 MPa. More than 50% of ULSD droplets are less than 50 μm under 1 MPa back pressure whereas the same accumulated probability (50%) corresponds to 75 μm under the atmospheric back pressure ($P_b = 0.1$ MPa). With the increase of the injection flow rate, the influence of back pressure on SMD weakens. When the mass flow rate is 16 kg/h, the SMD under 1.0 MPa is a little higher than that of 0.1 MPa.

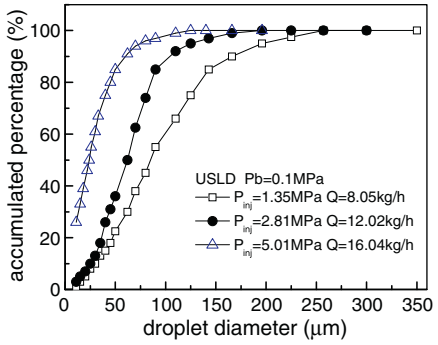

Fig. 8. Accumulated percentage of droplet size distribution for ULSD with different injection rates.

The SMD of diesel ejected from a pressure-swirl injector measured by Wang et al. (1987) [16] was 31.9 μm, with a flow rate of 16 kg/h and a pressure drop of 2.07 MPa, which is smaller than that of ULSD in this study due to the larger diameter of the injector nozzle in Wang et al. (1987) [16].

Fig. 8 shows the accumulated percentage of droplet size of ULSD under the back pressure of 0.1 MPa and different fuel injection rates (8, 12, and 16 kg/h respectively). It can be seen that the droplets at higher fuel flow rates are more uniform and gather at the zone with small droplets presenting better atomization. The accumulated percentage of droplet size less than 50 μm for ULSD is 75% when the injection rate is 16 kg/h, whereas the same droplet size ranges only accounts for 22.5% when the injection flow rate is 8 kg/h. Furthermore, with the increase of the injection flow rate of ULSD, the overall SMD of droplets decreases(57 μm, 14.5 μm for 8 kg/h, 16 kg/h respectively) due to the enhanced interaction between the fuel and surrounding field (seen Fig. 9b).

Fig. 9 shows the influence of different fuels on the accumulated percentage of droplets and SMD with different mass flow rates at a back pressure of 0.1 MPa and injection flow rate of 8 kg/h. It is obvious that the droplet size of DME is finer and its droplet size distribution is very uniform. 100% of the accumulated percentage of droplet size is below 25 μm. The better atomization quality is attributed to the special evaporation property of DME, which makes DME be in the flash boiling condition under a 0.1 MPa back pressure. In comparison to ULSD, methanol has a relatively smoother size distribution and 60% of the droplets are less than 25 μm, while 60% of ULSD droplets are less than 100 μm.

Fig. 9b shows that the SMD of ULSD is much more sensitive than that of other fuels. The main reason is the different thermo-properties of those three fuels. The viscosities and surface tensions of methanol and DME are much lower than those of ULSD. DME has the lowest surface

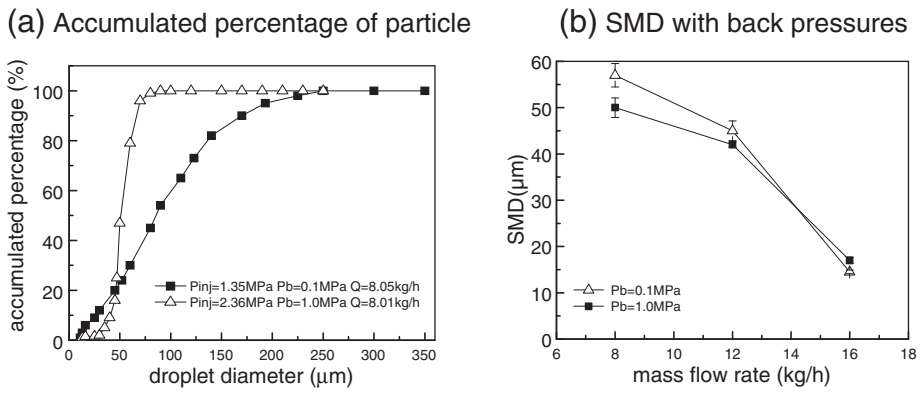

Fig. 7. Droplet size distributions and SMD of ULSD under different back pressures.

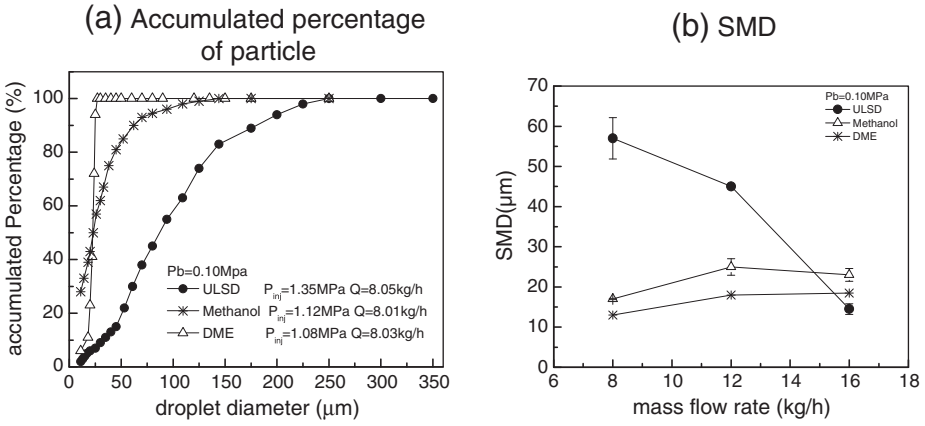

Fig. 9. The influence of fuels on size distribution and SMD (Pb = 0.1 MPa).

tension among the three fuels and its boiling point at atmospheric pressure is only −24.9 °C (the superheat temperature under room temperature is around 45 °C), which causes the flash boiling of DME spray under P_{atm}. Under normal back pressure, flash-boiling dominates the atomization of DME, and the droplet size is not sensitive to the mass flow rate of DME. Although under normal back pressure the methanol is mostly in liquid condition, its surface tension and kinematic viscosity are much lower than that of ULSD, which leads to the easier breakup of its droplets. Contrarily, ULSD has much larger surface tension and viscosity, and the breakup of its droplets is mainly due to aerodynamic forces, and convection effects.

Additionally, the SMDs of DME and methanol with different injection mass flow rates show similar variation.

Fig. 10 compares the accumulated percentage of droplet size and SMD with different mass flow rates along the same line referred above under the back pressure of 1.0 MPa and injection flow rate of 8 kg/h. It can be seen that ULSD and methanol follow the similar pattern of accumulated percentage while the size of DME under a back pressure of 1.0 MPa shows very different characteristics with large droplet size distribution. Around 75% (accumulated percentage) of DME droplets are less than 70 μm as opposed to 40 μm of ULSD at the same accumulated percentage. It indicates that high back pressure indeed has a negative effect on the atomization of DME. Furthermore, the SMD value of DME is much higher than that of methanol and ULSD. Interestingly, the SMD value of methanol is almost unchanging with injection flow rates while that of ULSD decreased with the increase of the injection flow rate.

4. Conclusions

In this article, the spray characteristics of methanol, DME and ULSD used in a Stirling engine were investigated systematically under different fuel flow rates and back pressures with a constant volume pressure vessel by high speed camera and FAM laser particle size analyzer. The results were compared and the following conclusions were drawn.

1) The injection pressure and ambient pressure had a prominent influence on the spray tip penetration and spray angles. During the initial period of spray, the lower speed of the liquid from nozzle under the small injection pressure have an obvious effect on the spray penetration rate indicating a slower penetration period (14 ms, 11 ms, 7 ms for 8 kg/h, 12 kg/h, 16 kg/h respectively). Higher injection pressure makes the spray grow fast whereas a higher pressure inside the pressure vessel leads to the decrease of spray penetration and the shrink of the spray angle.
2) The physical properties of ULSD, methanol and DME play important roles in their spray formation and atomization. Under atmospheric pressure, the spray of DME is in the flash-boiling condition. Its spray penetration rate is higher than that of ULSD and methanol but ULSD has the highest penetration rate at the start of injection under 2.2 MPa of back pressure and a 16 kg/h injection rate, whereas DME displays an opposite trend. When the spray stays at stable conditions, DME has the largest averaged spray angle of 29.1° followed by 26.5° of methanol and 21.6° of ULSD respectively.

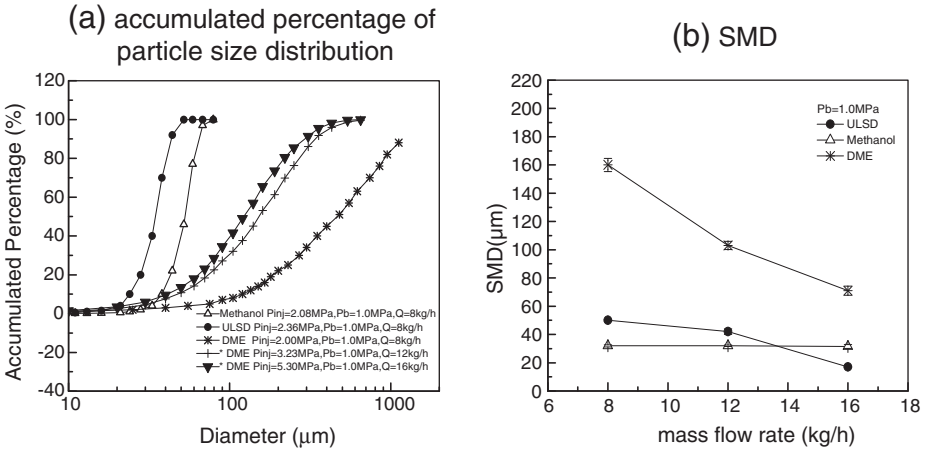

Fig. 10. The influence of fuels on droplet size distribution and SMD (Pb = 1.0 MPa).

3) The results also indicate that under atmospheric pressure and an injection rate of 8 kg/h, the size distribution of DME is very uniform and 100% accumulated percentage of droplets along the measurement line are below 25 μm. However, higher back pressures had a negative effect on the spray characteristics of the three kinds of fuels, especially DME. The SMD of DME is much higher than that of methanol and ULSD.

Acknowledgment

Authors would like to thank the National Natural Science Foundation of China (Grant No. 51176119 and 50976070) and Micropowers Ltd. of Shanghai for supporting this project. We also appreciate the effort of Dr. Dehao Ju on the proof reading of this paper.

References

[1] K. Sato, et al., Development of small-scale CHP plant with a wood powder-fueled Stirling engine, J. Power Energy Syst. 2 (5) (2008) 1221–1231.
[2] A. Nishiyama, et al., Fuel and emissions properties of Stirling engine operated with wood powder, Fuel 86 (15) (2007) 2333–2342.
[3] A. Pourmovahed, T. Opperman, B. Lemke, Performance and efficiency of a biogas CHP system utilizing a Stirling engine, Proceedings of the International Conference on Renewable Energies and Power Quality, Las Palmas de Gran Canaria, Spain, April, 2011.
[4] A.A. Aliabadi, et al., Efficiency and emissions measurement of a Stirling-engine-based residential microcogeneration system run on diesel and biodiesel, Energy Fuel 23 (2) (2009) 1032–1039.
[5] N. Farra, T. Tzanetakis, M.J. Thomson, Experimental determination of the efficiency and emissions of a residential microcogeneration system based on a Stirling engine and fueled by diesel and ethanol, Energy Fuel 26 (2) (2012) 889–900.
[6] C. Sayin, et al., Effect of injection timing on the exhaust emissions of a diesel engine using diesel–methanol blends, Renew. Energy 34 (5) (2009) 1261–1269.
[7] S.H. Park, H.J. Kim, C.S. Lee, Effects of dimethyl-ether (DME) spray behavior in the cylinder on the combustion and exhaust emissions characteristics of a high speed diesel engine, Fuel Process. Technol. 91 (5) (2010) 504–513.
[8] M.-R. Chao, et al., Effects of methanol-containing additive on emission characteristics from a heavy-duty diesel engine, Sci. Total Environ. 279 (1–3) (2001) 167–179.
[9] M. Yao, et al., Experimental study on the combustion process of dimethyl ether (DME), SAE Trans. 112 (4) (2003) 2422–2429.
[10] S.H. Yoon, J.P. Cha, C.S. Lee, An investigation of the effects of spray angle and injection strategy on dimethyl ether (DME) combustion and exhaust emission characteristics in a common-rail diesel engine, Fuel Process. Technol. 91 (11) (2010) 1364–1372.
[11] I.M. Youn, et al., Investigation on the fuel spray and emission reduction characteristics for dimethyl ether (DME) fueled multi-cylinder diesel engine with common-rail injection system, Fuel Process. Technol. 92 (7) (2011) 1280–1287.
[12] Z. Yusheng, et al., A Study on Combustion and Emission Characteristics of Small DI Diesel Engine Fuelled with Dimethyl Ether, 2005.
[13] C.H. Cheng, et al., Comparison of emissions of a direct injection diesel engine operating on biodiesel with emulsified and fumigated methanol, Fuel 87 (10–11) (2008) 1870–1879.
[14] R.H. Perry, D.W. Green, Perry's Chemical Engineers' Handbook, McGraw-Hill Professional Publishing, 2007.
[15] A.H. Lefebvre, Atomisation and Sprays, CRC Press, Taylor & Francis Group, Boca Raton, FL, USA, 1989.
[16] X. Wang, A. Lefebvre, Mean drop sizes from pressure-swirl nozzles, J. Propuls. Power 3 (1) (1987) 11–18.
[17] X. Wang, et al., Spray characteristics of high-pressure swirl injector fueled with methanol and ethanol, Energy Fuel 19 (6) (2005) 2394–2401.
[18] H.K. Suh, S.W. Park, C.S. Lee, Atomization characteristics of dimethyl ether fuel as an alternative fuel injected through a common-rail injection system, Energy Fuel 20 (4) (2006) 1471–1481.
[19] H.K. Suh, C.S. Lee, Experimental and analytical study on the spray characteristics of dimethyl ether (DME) and diesel fuels within a common-rail injection system in a diesel engine, Fuel 87 (6) (2008) 925–932.
[20] P.H. Mesman, B. Veenhuizen, The Spray Behavior of Liquid LPG at Different Back Pressures During Injection in a Constant Volume Chamber, SAE International, 2009.
[21] L.F. Moody, Friction factors for pipe flow, Trans. Asme 66 (8) (1944) 671–684.
[22] A.M. Duncan, et al., High-pressure viscosity of soybean-oil-based biodiesel blends with ultra-low-sulfur diesel fuel, Energy Fuel 26 (11) (2012) 7023–7036.
[23] C. Baumgarten, Mixture Formation in Internal Combustion Engines, Springer Berlin, Heidelberg, 2006.